

# Definitive Structural Identification toward Molecule-Type Sites within 1D and 2D Carbon-Based Catalysts

Hongliang Jiang, Qun He, Changda Wang, Hengjie Liu, Youkui Zhang, Yunxiang Lin, Xusheng Zheng, Shuangming Chen,\* Pulickel M. Ajayan, and Li Song\*

Developing facile preparation routes and atomic-level characterization methods for single-atom catalysts is highly desirable but still challenging. Herein, a general strategy is proposed to construct transition metal single atoms within 1D and 2D carbon supports. The carbon supports, typically graphene and carbon nanotubes, are coated with various transition metal-containing bimetal hydroxides, followed by polydopamine coating and high-temperature pyrolysis. X-ray absorption fine structure spectroscopy measurements and simulations efficiently indicate that single atoms (Co, Fe, or Cu) are captured within the applied carbon supports, distinctively forming exclusive molecule-type sites. As a proof-of-concept application, the obtained catalysts exhibit remarkable performance for electrochemical oxygen reduction reaction, even surpassing commercial Pt/C catalyst. The developed versatile route opens up new avenues for the design of carbon-based catalysts with definite molecular active sites. The atomic-level structural identifications provide significant guidance for mechanistic studies toward single-atom catalysts.

Recently, transition metal species supported onto carbon supports are being one of the research frontiers due to their distinctive catalytic properties in various catalytic reactions.<sup>[1–3]</sup> The size of the metal species is a key factor to determine the activities and efficiencies of these catalysts,<sup>[4,5]</sup> based on the fact that only the surface active-site atoms with unique low-coordination feature can be used in catalytic processes.<sup>[6,7]</sup> Therefore, downsizing the metal particles or clusters to single atoms is considered as valid methods to increase the efficiencies.<sup>[8,9]</sup> However, the high surface energy of small-size transition metals usually causes the aggregation.<sup>[10]</sup> In this regard, the introduction of the N atoms

as the “anchor” into the carbon supports is usually applied to stabilize the molecular metal species by bonding with N atoms, thus forming highly stable and well-dispersed metal-N-C molecular moieties.<sup>[11,12]</sup> Such molecular moieties dispersed carbon-based catalysts are usually evolved from the pyrolysis of ideal metal complexes with rigorous macrocyclic N<sub>4</sub> ligands, which surely limits the selectivity of precursors and structural maneuverability of the designed catalysts.<sup>[9,13]</sup> On the other hand, these molecular moieties are extensively demonstrated as the catalytically active sites for a series of catalytic reactions, such as hydrogen evolution,<sup>[14,15]</sup> CO<sub>2</sub> reduction,<sup>[16,17]</sup> oxygen reduction,<sup>[9,18]</sup> and so on. Thus, the realization of the structural identifications with atomic-level precision toward these molecular moieties is highly desirable to unravel the intrinsic mechanism, but still keeping as a great challenge.

We here demonstrated, for the first time, one general space-confinement strategy to achieve highly dispersed transition metal single atoms within typical graphene and carbon nanotubes supports (see the Supporting Information for details). As illustrated in **Figure 1**, homogeneous ZnM (M = Co, Fe, or Cu) dual-metal hydroxides layers were first in situ synthesized onto graphene oxide (GO) or acid-treated multiwalled carbon nanotubes (MWCNTs) using a simple hydrolysis method (Figure S1, Supporting Information) with low hydrolysis rate (denoted as ZnM(OH)<sub>x</sub>@GO and ZnM(OH)<sub>x</sub>@MWCNTs, respectively). Then the obtained composites were further coated with polydopamine (PDA) as N-rich carbon precursors (denoted as PDA@ZnM(OH)<sub>x</sub>@GO and PDA@ZnM(OH)<sub>x</sub>@MWCNTs, respectively). The final products were obtained through thermal treatment of the above precursors to pyrolyze PDA and remove the metal zinc (noted as M<sub>1</sub>@N-doped graphene and M<sub>1</sub>@N-doped MWCNTs). Systematic characterizations, especially X-ray absorption fine structure spectroscopy and aberration-corrected scanning transmission electron microscopy (AC-STEM), were performed to characterize the fine structures of as-prepared samples. As demonstrated, these samples were applied as catalysts for oxygen reduction reaction (ORR), and the catalytic activities and stabilities were elaborately evaluated. Our work provides new opportunities to synthesize single atoms supported catalysts, and it is believed that this general method can be extensively used to synthesize other related catalysts.

Dr. H. Jiang, Q. He, C. Wang, H. Liu, Y. Zhang, Y. Lin, Dr. X. Zheng, Dr. S. Chen, Prof. L. Song  
National Synchrotron Radiation Laboratory  
CAS Center for Excellence in Nanoscience  
University of Science and Technology of China  
Hefei, Anhui 230029, China  
E-mail: csmp@ustc.edu.cn; song2012@ustc.edu.cn

Prof. P. M. Ajayan  
Department of Science and Technology of China  
Rice University  
Houston, TX 77005, USA

The ORCID identification number(s) for the author(s) of this article can be found under <https://doi.org/10.1002/aenm.201800436>.

DOI: 10.1002/aenm.201800436

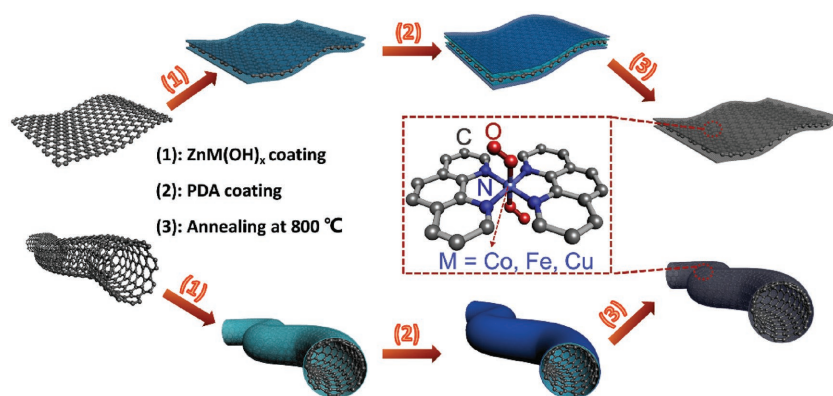


**Figure 1.** Schematic illustration of the synthesis processes for molecule-type metal-N-C materials supported on graphene and MWCNTs.

Taking  $\text{Co}_1@N$ -doped graphene as an example, a series of characterizations were conducted. The GO as the substrate was synthesized by a modified Hummers' method.<sup>[19]</sup> The X-ray diffraction (XRD) patterns and scanning electron microscopy image indicate the characteristic interlayer stacking structure of GO with an interlayer spacing of  $\approx 0.8$  nm and a typical sheet-like morphology (Figure S2, Supporting Information). After loading dose-setting  $\text{ZnCo}(\text{OH})_x$  coating layers (Figure S3a, Supporting Information) onto the GO substrate via a propylene oxide-mediated alkalization method,<sup>[20]</sup> GO-like morphology without separate components and homogeneous distribution of Zn and Co element are observed (Figure S3b,c, Supporting Information), confirming the uniform ZnCo bimetal hydroxides coating onto the GO according to previous reports about ZnCo hydroxides.<sup>[21,22]</sup> The uniform coating is the key to realize subsequent efficient PDA coating and prevent the structural changes. As expected, negligible morphology changes and no sign of free PDA suggest the perfect PDA coating (Figure S3d, Supporting Information). The ideal bimetal hydroxides and PDA coating layers are supposed to synthesize designed structures with monodispersed metal species under high temperature pyrolysis. The consistent results are also observed in the preparation processes of Fe and Cu-containing composites as well as the MWCNTs-based samples (Figures S4–S8, Supporting Information), indicating that both the employed methods for the bimetal hydroxides and PDA coating are versatile and could be extended to other transition metals and 1D carbon supports. Notably, the effects of the Zn species and PDA layers on the formation of single metal atoms within carbon supports would be deeply discussed in the following section.

These above samples with coating layers were pyrolyzed under flowing  $\text{N}_2$  at  $800^\circ\text{C}$ . The high-temperature treatment led to the PDA decomposition and conversion to N-doped carbon layers, thus providing anchor sites for metal species.<sup>[23]</sup> Besides, the bimetal hydroxides would be reduced to form  $M-N_x$  sites, in which zinc would be evaporated out due to its low boiling point (mp  $420^\circ\text{C}$ , bp  $907^\circ\text{C}$ ).<sup>[12]</sup> The XRD patterns of the  $\text{Co}_1@N$ -doped graphene show that no Co-related diffraction peaks can be observed, similar with that of N-doped graphene without adding metal precursors. Similar XRD results are also observed for  $\text{Fe}_1@N$ -doped graphene,  $\text{Cu}_1@N$ -doped graphene, and  $\text{Co}_1@N$ -doped MWCNTs (Figure S9, Supporting Information).

These results imply that the metal species in the  $M_1@N$ -doped graphene and  $M_1@N$ -doped MWCNTs probably are highly dispersed or sufficiently small. In contrast, as for PDA-free ( $\text{ZnCo}(\text{OH})_x@GO$ ) or Zn-free precursors ( $\text{PDA}@Co(\text{OH})_x@GO$ ) derived samples, obvious metal Co components are generated (marked as Co NPs@graphene and Co NPs@N-doped graphene, respectively), as revealed by XRD patterns (Figure S10, Supporting Information and Figure 2a). The above results were further proved by the direct observations from transmission electron microscopy (TEM). Figure 2b shows the TEM image of  $\text{Co}_1@N$ -doped graphene, in which no obvious Co nanoparticles can be observed. The corresponding selected area

electron diffraction (SAED) pattern suggests its poor crystallinity (the inset of Figure 2b). The consistent observations are also exhibited for  $\text{Fe}_1@N$ -doped graphene,  $\text{Cu}_1@N$ -doped graphene, and  $\text{Co}_1@N$ -doped MWCNTs (Figure S11, Supporting Information). These images are similar with that of the metal-free sample (N-doped graphene, Figure S12, Supporting Information). However, obvious nanoparticles can be seen in the TEM images of Co NPs@graphene and Co NPs@N-doped graphene (Figure S13, Supporting Information), demonstrating the important roles of PDA coating layers and metal zinc in inhibiting aggregation and crystal growth. The effects of PDA and Zn species are similar with that of organic ligands and Zn atoms in bimetallic Zn/Co metal-organic frameworks for the preparation of Co single atoms.<sup>[10]</sup> To further state the existed form of Co, the aberration-corrected atomic-resolution high-angle annular dark-field (HAADF) STEM was carried out. The obviously bright dots could be attributed to the Co atoms due to its relatively large Z-value,<sup>[24]</sup> demonstrating the monodispersed property of Co atoms on the substrate (Figure 2c). The corresponding energy-dispersive X-ray (EDX) mapping analysis indicates the homogeneous distribution of N and Co into the graphene substrate (Figure 2d). The monodispersed Co atoms and elemental mapping measurement for  $\text{Co}_1@N$ -doped MWCNTs by HAADF-STEM are similar with  $\text{Co}_1@N$ -doped graphene (Figure S14, Supporting Information). The inductively coupled plasma mass spectroscopy analysis reveals the Co content of  $\approx 2.1$  wt% and complete removal of the Zn species in the  $\text{Co}_1@N$ -doped graphene. X-ray photoelectron spectroscopy measurement indicates that the N content is  $\approx 3.62$  at% (Figure S15a, Supporting Information). The high-resolution N 1s spectrum (Figure S15b, Supporting Information) suggests that the N species mainly form into pyridinic-N and graphitic-N which could serve as active sites of some electrochemical reactions and the anchor sites of metal species. Additionally, the Raman result (Figure S16, Supporting Information) implies the existence of structural defects probably due to the introduction of the metal-N moieties.

Although the above results have suggested that these metal species forming single atoms exist within the graphene and MWCNTs supports, the precise coordination environments are needed to further be dissected due to great significance for unraveling the catalytic mechanism.<sup>[16–18]</sup> We performed X-ray absorption near-edge structure (XANES) and extended X-ray absorption

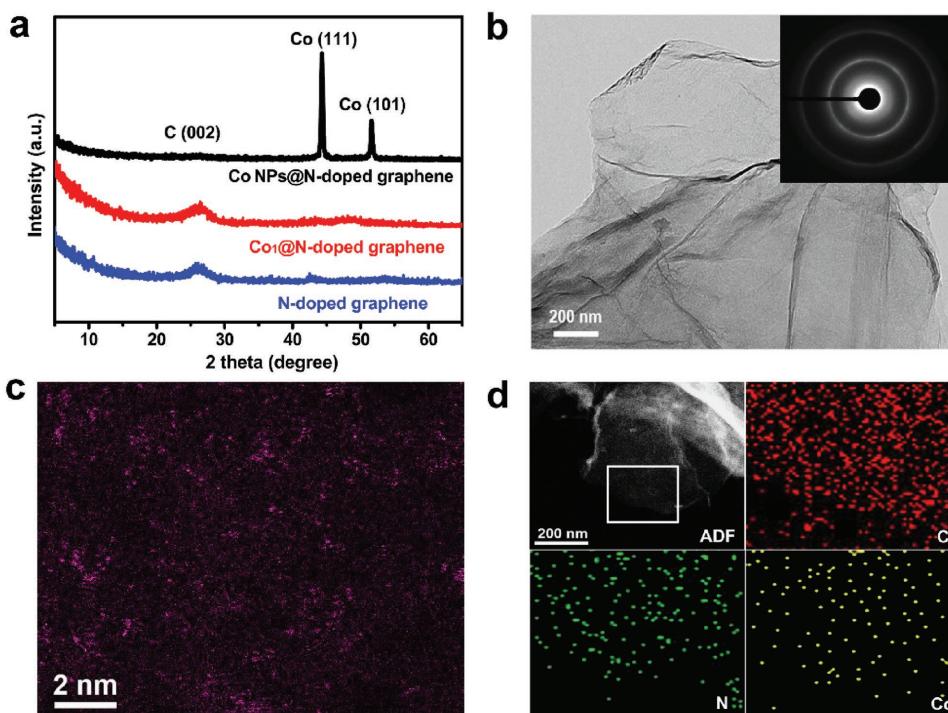


**Figure 2.** a) XRD patterns of N-doped graphene,  $\text{Co}_1$ @N-doped graphene, and Co NPs@N-doped graphene. b) TEM image of  $\text{Co}_1$ @N-doped graphene (inset: SAED image). c) Aberration-corrected magnified HAADF-STEM image of  $\text{Co}_1$ @N-doped graphene. d) ADF image and corresponding EDX mapping of  $\text{Co}_1$ @N-doped graphene.

fine structure (EXAFS) measurements. The XANES curve of  $\text{Co}_1$ @N-doped graphene shows that the near-edge adsorption energy locates among those of Co foil, CoPc, and CoO, implying that Co atoms are positively charged (Figure 3a). Similar results are also observed in the XANES curves of  $\text{Fe}_1$ @N-doped graphene,  $\text{Cu}_1$ @N-doped graphene, and related control samples (Figure S17, Supporting Information). Further structural information about Co atoms can be obtained from the EXAFS. As exhibited, the  $\text{Co}_1$ @N-doped graphene shows a similar oscillation curve with CoPc in k-space (Figure 3b), suggesting that the main structure of Co atoms in  $\text{Co}_1$ @N-doped graphene is  $\text{Co-N}_4$  coordination. Similar results are also observed in the k-space curves of  $\text{Fe}_1$ @N-doped graphene,  $\text{Cu}_1$ @N-doped graphene (Figure S18, Supporting Information), indicating the consistent  $\text{M-N}_4$  coordination structures of these metal species.<sup>[23]</sup> The Fourier-transformed  $k^3$ -weighted EXAFS R-space spectrum of  $\text{Co}_1$ @N-doped graphene only shows one noticeable peak in the region 1–2 Å with similar bond length of CoPc (Figure 3c). This result strongly suggests that Co–N coordination is separately formed without the metal–metal bonds.<sup>[12]</sup> The similar Fe–N and Cu–N coordination are also observed from Fe and Cu K-edge EXAFS results (Figure S19, Supporting Information). Furthermore, the wavelet transformation (WT) was analyzed to show the Co K-edge EXAFS oscillations. As displayed in Figure 3d, the maximum center at  $\approx 5.3 \text{ \AA}^{-1}$  for  $\text{Co}_1$ @N-doped graphene could be assigned to the Co–N bonds,<sup>[25]</sup> and no Co–Co maximum center is observed, as revealed by the comparison with the WT plots of CoO and Co foil in Figure 3e,f. Notably, the WT plots of  $\text{Co}_1$ @N-doped graphene and CoPc possess some difference (Figure 3d,g). Therefore, it inspires us to dissect the Co-related structures in  $\text{Co}_1$ @N-doped graphene. Consequently, based on typical  $\text{Co-N}_4$  coordination, possible

structure of Co species in  $\text{Co}_1$ @N-doped graphene is rationally established. The detailed structure models and corresponding calculated theoretical XANES spectra are displayed in Figure 3h and Figure S20 in the Supporting Information. Interestingly, the structure with two oxygen molecules weakly adsorbed on the Co atoms of  $\text{Co-N}_4$  coordination could match well with the main features of the experimental spectrum for  $\text{Co}_1$ @N-doped graphene (Figure 3h). The WT plots and theoretical spectra of Fe and Cu-containing materials are also calculated and show similar results with that of Co-containing ones (Figures S21–S24, Supporting Information). Based on the above results, exclusive molecule-type sites (the inset of Figure 3h, denoted as  $\text{MN}_4\text{C}_8\text{O}_2$ ,  $\text{M} = \text{Co}, \text{Fe}, \text{Cu}$ ) are efficiently captured within the applied carbon supports.

As evidenced by recent reports, such structure with mono-dispersed transition metal atoms could serve as highly active sites for electrocatalysis.<sup>[8,25]</sup> The N species and metal–N sites could favor the rate-limiting  $\text{O}_2$  activation for ORR.<sup>[9,12]</sup> Thus, as a proof-of-concept application, the ORR performance of the obtained materials was evaluated in  $\text{O}_2$ -saturated 0.1 M KOH electrolyte. The ORR activities of  $\text{Co}_1$ @N-doped graphene were first investigated. The cyclic voltammetry (CV) curve of  $\text{Co}_1$ @N-doped graphene shows no obvious featured peaks in the  $\text{N}_2$ -saturated KOH solution, while a well-defined cathodic peak toward ORR is observed in  $\text{O}_2$ -saturated KOH solution, indicating distinct ORR activity of the catalyst (Figure 4a).<sup>[26,27]</sup> Similar cathodic peaks are also observed in the CVs of other single metal atoms-containing catalysts (Figure S25, Supporting Information). The linear sweep voltammetry (LSV) curves (Figure 4b) indicate that  $\text{Co}_1$ @N-doped graphene shows the impressive activities in terms of the positive onset ( $E_{\text{onset}}$ ) and half-wave potential ( $E_{1/2}$ ). As shown in Figure 4b, the  $E_{1/2}$  of

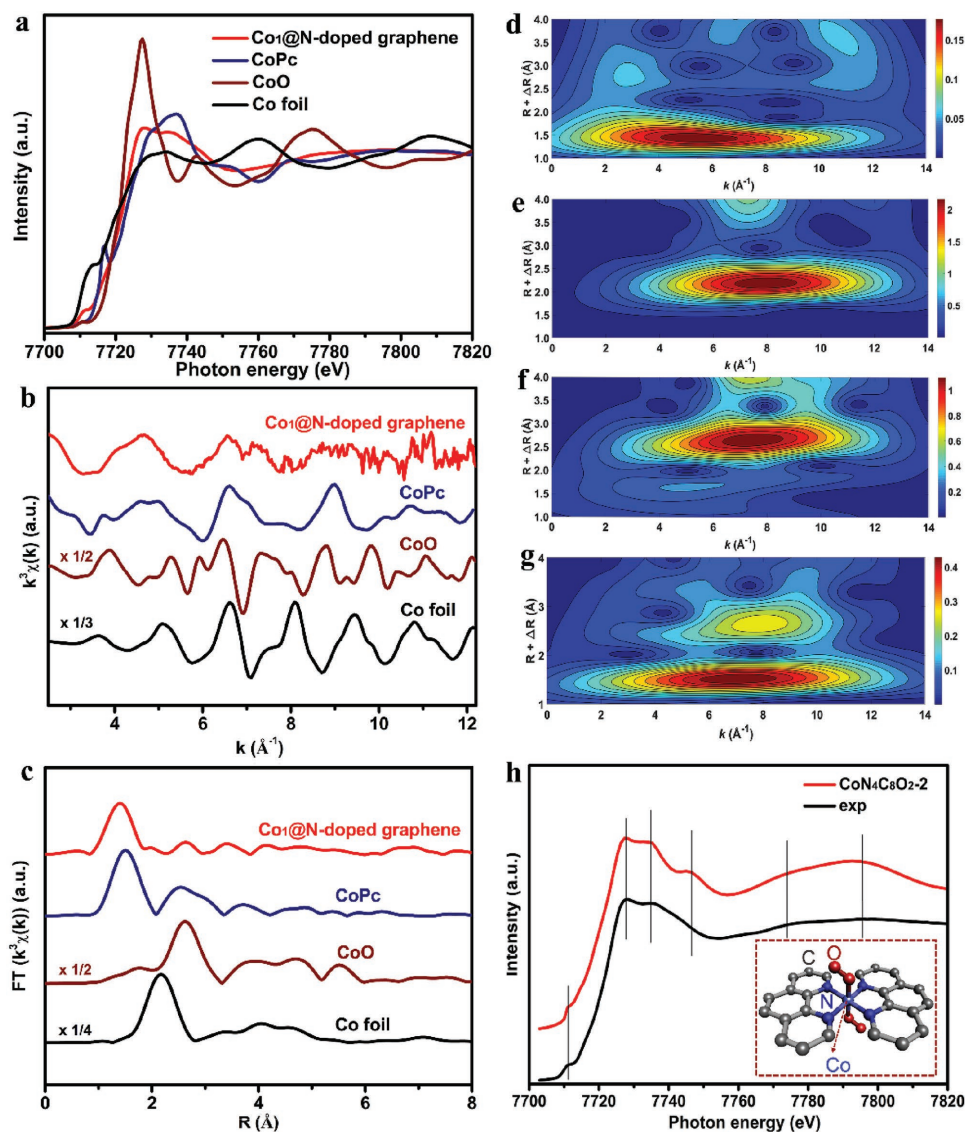


**Figure 3.** a) Co K-edge XANES curves and b) EXAFS curves at k-space and c) R-space of Co<sub>1</sub>@N-doped graphene, CoPc, CoO, and Co foil. d) WT of Co<sub>1</sub>@N-doped graphene, e) Co foil, f) CoO, and g) CoPc. h) The comparison between the normalized Co K-edge XANES experimental spectrum and the theoretical spectrum calculated based on the inset structure.

Co<sub>1</sub>@N-doped graphene is 0.865 V versus reversible hydrogen electrode (RHE), which is 15 mV more positive than that of Pt/C catalyst and 105 mV larger than that of the metal-free sample. The  $E_{1/2}$  is comparable to that of most nonprecious metal ORR electrocatalysts (Table S1, Supporting Information). LSV measurements were also recorded at different rotation rates (Figure S26, Supporting Information). The value of electron transfer number ( $n$ ) was calculated by the rotating ring disk electrode (RRDE) test (Figure S27, Supporting Information). The calculated electron transfer number surpasses 3.8 in the range of 0.2–0.8 V versus RHE, demonstrating a near four-electron ORR pathway for the Co<sub>1</sub>@N-doped graphene (Figure 4c). The corresponding H<sub>2</sub>O<sub>2</sub> yield calculated from RRDE over Co<sub>1</sub>@N-doped graphene remains below 4% at the wide potential range. These results strongly prove that the Co<sub>1</sub>@N-doped graphene electrode exhibits high ORR catalytic efficiency. As

for other M<sub>1</sub>@N-doped MWCNTs and M<sub>1</sub>@N-doped graphene catalysts, the impressive ORR performance is also obtained (Figures S28–S30, Supporting Information). Furthermore, The ORR performance of the Co<sub>1</sub>@N-doped graphene catalyst in acidic media was evaluated. From the  $E_{\text{onset}}$  and  $E_{1/2}$  of the polarization curves (Figure S31, Supporting Information), it could be concluded that the Co<sub>1</sub>@N-doped graphene catalyst shows promising potentials in the proton exchange membrane fuel cell.

The electrocatalytic durability of these catalysts is also evaluated. The high stability of Co<sub>1</sub>@N-doped graphene is proved by the long-term CVs and chronoamperometry measurements, in which very low negative  $E_{1/2}$  shift or current decline are achieved, superior to Pt/C (Figure 4d and Figures S32 and S33, Supporting Information). To examine the fuel crossover effect,<sup>[28,29]</sup> the Co<sub>1</sub>@N-doped graphene as well as Pt/C was tested in both O<sub>2</sub>-saturated 0.1 M KOH and O<sub>2</sub>-saturated 0.1 M KOH with 1.0 M methanol

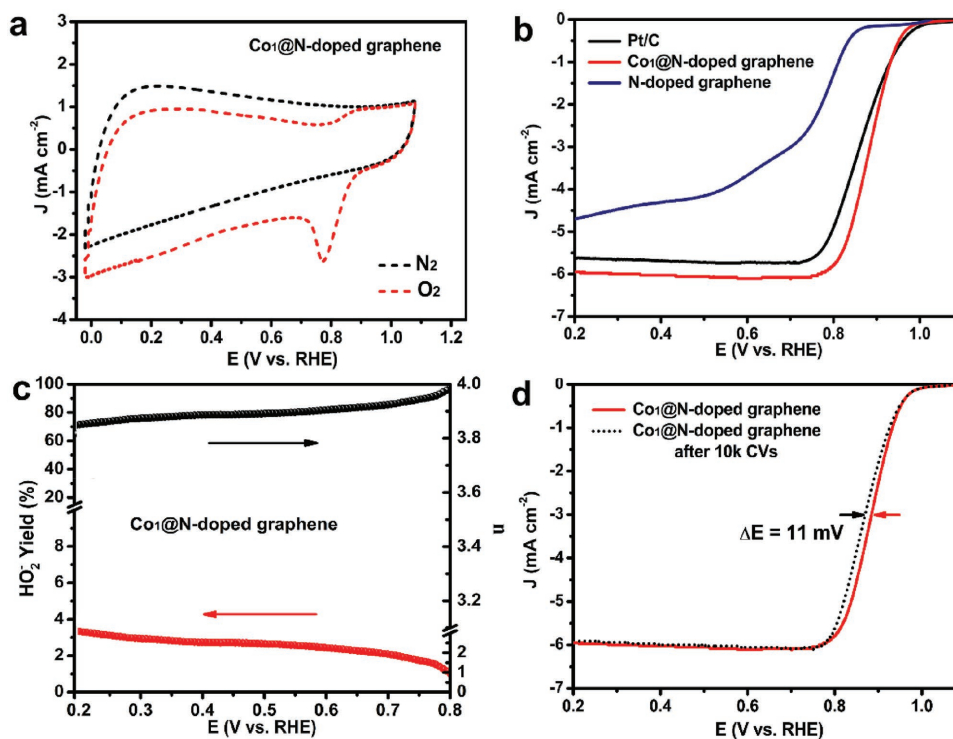


**Figure 4.** a) CVs of Co<sub>1</sub>@N-doped graphene in O<sub>2</sub> and N<sub>2</sub>-saturated 0.1 M KOH solution. b) ORR polarization curves of Co<sub>1</sub>@N-doped graphene, Pt/C and N-doped graphene. c) Electron transfer number ( $n$ ) and H<sub>2</sub>O<sub>2</sub> yield versus potential (%) calculated from RRDE measurements. d) LSV curves of Co<sub>1</sub>@N-doped graphene before and after 10000 potential cycles in O<sub>2</sub>-saturated 0.1 M KOH.

solutions. There is no obvious change in the current density for Co<sub>1</sub>@N-doped graphene after adding 1.0 M methanol into the solution (inset in Figure S32, Supporting Information); however, the current density apparently vanished for Pt/C (inset in Figure S33, Supporting Information). The above results reveal that Co<sub>1</sub>@N-doped graphene has promising tolerance to methanol crossover. The excellent durability and methanol tolerance of other catalysts are also proved (Figures S34–S36, Supporting Information).

In summary, we have successfully proposed a versatile space-confinement route for the synthesis of single transition metal atoms within graphene and carbon nanotubes supports. More importantly, the elaborate X-ray absorption spectra analysis efficiently demonstrated that these single atoms form exclusive molecule-type sites (MN<sub>4</sub>C<sub>8</sub>O<sub>2</sub>-2, M = Co, Fe, Cu). The excellent ORR performance of these molecular metal-N-C catalysts highlights the importance of the developed strategy on the design of molecule-type catalysts for the mechanistic insights and practical applications in electrocatalytic field.

## Supporting Information

Supporting Information is available from the Wiley Online Library or from the author.

## Acknowledgements

H.J. and Q.H. contributed equally to this work. This work was financially supported by Ministry of Science and Technology of China

(2017YFA0303500 and 2014CB848900), National Natural Science Foundation of China (U1532112, 11574280, 11605201, and 21706248), Chinese Academy of Sciences (CAS) Key Research Program of Frontier Sciences (QYZDB-SSW-SLH018), China Postdoctoral Science Foundation (BH2310000033), CAS Interdisciplinary Innovation Team, Innovative Program of Development Foundation of Hefei Center for Physical Science (T6FXCX003). L.S. acknowledges the recruitment program of global experts, the CAS Hundred Talent Program, Key Laboratory of Advanced Energy Materials Chemistry (Ministry of Education) Nankai University (111 project, B12015), Key Laboratory of the Ministry of Education for Advanced Catalysis Materials and Zhejiang Key Laboratory for Reactive Chemistry on Solid Surfaces (Zhejiang Normal University). The authors thank the Shanghai Synchrotron Radiation Facility (14W1, SSRF), the Beijing Synchrotron Radiation Facility (1W1B and soft-X-ray endstation, BSRF), the Hefei Synchrotron Radiation Facility (Photoemission, Magnetic Circular Dichroism and Catalysis/Surface Science Endstations, National Synchrotron Radiation Laboratory), and the University of Science and Technology of China Center for Micro and Nanoscale Research and Fabrication for helps in characterizations.

## Conflict of Interest

The authors declare no conflict of interest.

## Keywords

carbon supports, electrocatalysts, oxygen reduction reaction, single atoms, X-ray absorption spectroscopy

Received: February 7, 2018

Revised: March 8, 2018

Published online:

- [1] W. Liu, L. Zhang, X. Liu, X. Liu, X. Yang, S. Miao, W. Wang, A. Wang, T. Zhang, *J. Am. Chem. Soc.* **2017**, *139*, 10790.
- [2] H. T. Chung, D. A. Cullen, D. Higgins, B. T. Sneed, E. F. Holby, K. L. More, P. Zelenay, *Science* **2017**, *357*, 479.
- [3] R. V. Jagadeesh, K. Murugesan, A. S. Alshammari, H. Neumann, M.-M. Pohl, J. Radnik, M. Beller, *Science* **2017**, *358*, 326.
- [4] M. Crespo-Quesada, A. Yarulin, M. Jin, Y. Xia, L. Kiwi-Minsker, *J. Am. Chem. Soc.* **2011**, *133*, 12787.
- [5] B. Yoon, H. Häkkinen, U. Landman, A. S. Wörz, J. M. Antonietti, S. Abbet, K. Judai, U. Heiz, *Science* **2005**, *307*, 403.
- [6] X.-F. Yang, A. Wang, B. Qiao, J. Li, J. Liu, T. Zhang, *Acc. Chem. Res.* **2013**, *46*, 1740.
- [7] J. Huang, J. Chen, T. Yao, J. He, S. Jiang, Z. Sun, Q. Liu, W. Cheng, F. Hu, Y. Jiang, Z. Pan, S. Wei, *Angew. Chem., Int. Ed.* **2015**, *54*, 8722; *Angew. Chem.* **2015**, *127*, 8846.
- [8] X. Li, W. Bi, M. Chen, Y. Sun, H. Ju, W. Yan, J. Zhu, X. Wu, W. Chu, C. Wu, Y. Xie, *J. Am. Chem. Soc.* **2017**, *139*, 14889.
- [9] J. Wang, Z. Huang, W. Liu, C. Chang, H. Tang, Z. Li, W. Chen, C. Jia, T. Yao, S. Wei, Y. Wu, Y. Li, *J. Am. Chem. Soc.* **2017**, *139*, 17281.
- [10] W. Zhan, Q. He, X. Liu, Y. Guo, Y. Wang, L. Wang, Y. Guo, A. Y. Borisevich, J. Zhang, G. Lu, S. Dai, *J. Am. Chem. Soc.* **2016**, *138*, 16130.
- [11] C. Tang, B. Wang, H. F. Wang, Q. Zhang, *Adv. Mater.* **2017**, *29*, 1703185.
- [12] P. Yin, T. Yao, Y. Wu, L. Zheng, Y. Lin, W. Liu, H. Ju, J. Zhu, X. Hong, Z. Deng, G. Zhou, S. Wei, Y. Li, *Angew. Chem., Int. Ed.* **2016**, *55*, 10800; *Angew. Chem.* **2016**, *128*, 10958.
- [13] C. Zhao, X. Dai, T. Yao, W. Chen, X. Wang, J. Wang, J. Yang, S. Wei, Y. Wu, Y. Li, *J. Am. Chem. Soc.* **2017**, *139*, 8078.
- [14] W. Chen, J. Pei, C. T. He, J. Wan, H. Ren, Y. Zhu, Y. Wang, J. Dong, S. Tian, W. C. Cheong, S. Lu, L. Zheng, X. Zheng, W. Yan, Z. Zhuang, C. Chen, Q. Peng, D. Wang, Y. Li, *Angew. Chem., Int. Ed.* **2017**, *56*, 16086; *Angew. Chem.* **2017**, *129*, 16302.
- [15] H. Fei, J. Dong, M. J. Arellano-Jimenez, G. Ye, N. Dong Kim, E. L. Samuel, Z. Peng, Z. Zhu, F. Qin, J. Bao, M. J. Yacaman, P. M. Ajayan, D. Chen, J. M. Tour, *Nat. Commun.* **2015**, *6*, 8668.
- [16] Y. Han, Y. G. Wang, W. Chen, R. Xu, L. Zheng, J. Zhang, J. Luo, R. A. Shen, Y. Zhu, W. C. Cheong, C. Chen, Q. Peng, D. Wang, Y. Li, *J. Am. Chem. Soc.* **2017**, *139*, 17269.
- [17] W. Ju, A. Bagger, G. P. Hao, A. S. Varela, I. Sinev, V. Bon, B. Roldan Cuenya, S. Kaskel, J. Rossmeisl, P. Strasser, *Nat. Commun.* **2017**, *8*, 944.
- [18] A. Zitolo, N. Ranjbar-Sahraie, T. Mineva, J. Li, Q. Jia, S. Stamatina, G. F. Harrington, S. M. Lyth, P. Krtil, S. Mukerjee, E. Fonda, F. Jaouen, *Nat. Commun.* **2017**, *8*, 957.
- [19] L. Peng, P. Xiong, L. Ma, Y. Yuan, Y. Zhu, D. Chen, X. Luo, J. Lu, K. Amine, G. Yu, *Nat. Commun.* **2017**, *8*, 15139.
- [20] B. Zhang, X. Zheng, O. Voznyy, R. Comin, M. Bajdich, M. García-Melchor, L. Han, J. Xu, M. Liu, L. Zheng, F. P. García de Arquer, C. T. Dinh, F. Fan, M. Yuan, E. Yassitepe, N. Chen, T. Regier, P. Liu, Y. Li, P. De Luna, A. Janmohamed, H. L. Xin, H. Yang, A. Vojvodic, E. H. Sargent, *Science* **2016**, *352*, 333.
- [21] D. Tang, Y. Han, W. Ji, S. Qiao, X. Zhou, R. Liu, X. Han, H. Huang, Y. Liu, Z. Kang, *Dalton Trans.* **2014**, *43*, 15119.
- [22] M. A. Woo, M.-S. Song, T. W. Kim, I. Y. Kim, J.-Y. Ju, Y. S. Lee, S. J. Kim, J.-H. Choy, S.-J. Hwang, *J. Mater. Chem.* **2011**, *21*, 4286.
- [23] M. Zhang, Y. G. Wang, W. Chen, J. Dong, L. Zheng, J. Luo, J. Wan, S. Tian, W. C. Cheong, D. Wang, Y. Li, *J. Am. Chem. Soc.* **2017**, *139*, 10976.
- [24] Y. Chen, S. Ji, Y. Wang, J. Dong, W. Chen, Z. Li, R. Shen, L. Zheng, Z. Zhuang, D. Wang, Y. Li, *Angew. Chem., Int. Ed.* **2017**, *56*, 6937; *Angew. Chem.* **2017**, *129*, 7041.
- [25] K. Jiang, S. Siahrostami, A. J. Akey, Y. Li, Z. Lu, J. Lattimer, Y. Hu, C. Stokes, M. Gangishetty, G. Chen, Y. Zhou, W. Hill, W.-B. Cai, D. Bell, K. Chan, J. K. Nørskov, Y. Cui, H. Wang, *Chemistry* **2017**, *3*, 950.
- [26] H. Jiang, Y. Yao, Y. Zhu, Y. Liu, Y. Su, X. Yang, C. Li, *ACS Appl. Mater. Interfaces* **2015**, *7*, 21511.
- [27] H. Jiang, Y. Su, Y. Zhu, J. Shen, X. Yang, Q. Feng, C. Li, *J. Mater. Chem. A* **2013**, *1*, 12074.
- [28] L. Shang, H. Yu, X. Huang, T. Bian, R. Shi, Y. Zhao, G. I. N. Waterhouse, L. Z. Wu, C. H. Tung, T. Zhang, *Adv. Mater.* **2016**, *28*, 1668.
- [29] H. Yu, L. Shang, T. Bian, R. Shi, G. I. N. Waterhouse, Y. Zhao, C. Zhou, L. Z. Wu, C. H. Tung, T. Zhang, *Adv. Mater.* **2016**, *28*, 5080.